J Solid State Electrochem (2001) 6: 39–54
DOI 10.1007/s100080000176

ORIGINAL PAPER

G. Patermarakis · K. Moussoutzanis · J. Chandrinos

Discovery by kinetic studies of the latent physicochemical processes and their mechanisms during the growth of porous anodic alumina films in sulfate electrolytes

Received: 19 July 2000 / Accepted: 4 October 2000 / Published online: 16 May 2001

Abstract The kinetics of growth of porous anodic alumina films in pure H_2SO_4, in mixtures of H_2SO_4 and $Al_2(SO_4)_3$ and in $Al(HSO_4)_3$, $NaHSO_4$ and $KHSO_4$ electrolytes were studied. The latent physicochemical processes at the pore base surface/electrolyte interface, across the barrier layer, inside the metal/oxide interface and at the pore wall surface/electrolyte interface and their mechanisms were revealed. High field strength equations were formulated describing the ionic migrations from the pore base surface. These showed that, at constant current density and temperature, the inverse of the pore base square diameter depends linearly on the inverse of the H^+ activity in the anodizing solution and that this diameter increases with H^+ activity, in agreement with the experimental results. The mechanism of electrolyte anion incorporation inside the barrier layer and the real distribution of the anion concentration across both the barrier layer and pore walls were deduced. The effects of the different kinds and concentrations of the electrolyte anions and cations on both the above processes and their mechanisms were also examined.

Keywords Aluminum anodizing · Sulfate electrolytes · Porous oxide growth kinetics · Latent physicochemical processes · Mechanisms

Abbreviations and symbols a_1: activation (half-jump) distance for the migration of OH^- ions · a_2: activation (half-jump) distance for the migration of O^{2-} ions · a_{H+}: activity of H^+ in solution · a_{OH-}: activity of OH^- in solution · $a_{OH-,b/d}$: activity of OH^- in the barrier layer/double layer (b/d) interface · b: $a_{OH-,b/d}$–a_{OH-} · C_{H2SO4}: concentration of H_2SO_4 in the bath solution · $C_{Al2(SO4)3}$: concentration of $Al_2(SO_4)_3$ in the bath solution · $C_{OH-,b/d}$: concentration of OH^- in the barrier layer/double layer (b/d) interface · COR: correlation coefficient · d_c: density of the compact pore wall oxide · D: average pore diameter at a distance h from the pore base · D_b: pore base diameter · D_c: cell size · $\Delta H°$: enthalpy of formation · ΔP_b: potential drop across the barrier layer · ΔP_f: potential drop across the entire film · ΔP_p: potential drop across the porous layer · $\Delta P_{p,h}$: potential drop along the pores of a film with thickness h · $\Delta P_{p,hc}$: potential drop along the pores of a film with thickness h_c · E_a: average field strength across the barrier layer · E_b: field strength on the pore base surface · E_r: relative field strength · F: $(kjt–m)(4^{-1}\pi S_g d_c\ k't)^{-1} = F_0 + F_1 t + F_2 t^2$ = dimensionless factor · F_0: $nD_b{}^2$ · F_1: parameter depending on the conditions inside the pores and the nature/composition and reactivity of the pore wall oxide · F_2: parameter depending on the conditions inside the pores and the nature/composition and reactivity of the pore wall oxide · F_c: Faraday's constant · h: film thickness · h_c: maximum limiting film thickness achieved on prolonged anodization · θ_{Al3+}: surface fraction of all the Al^{3+} ions · $\theta_{Al3+,b}$: surface fraction of the bare Al^{3+} ions not occupied by OH^- · θ_{OH-}: surface fraction of the Al^{3+} occupied by OH^- · θ_{O2-}: surface fraction of the O^{2-} ions · IEP: isoelectric point · j: current density · J_{O2-}: rate of migration of O^{2-} ions which reach the metal/oxide interface · J_{OH-}: rate of migration of OH^- ions which leave the pore base surface · J_{H+}: rate of the H^+ rejection in the pore base filling solution · $j_{O2-,t}$: $2J_{O2-}S_g^{-1}(2^{-1}\pi n D_b{}^2)^{-1}$ = true ionic current density referred to the migration of the O^{2-} ions from the pore base surface · $j_{OH-,t}$: $J_{OH-}S_g^{-1}(2^{-1}\pi n D_b{}^2)^{-1}$ = true ionic current density referred to the migration of the OH^- ions from the pore base surface · k: constant for oxide production resulting from Faraday's law · k': $k''j$ = rate of the film thickness growth · k'': constant

G. Patermarakis (✉) · K. Moussoutzanis · J. Chandrinos
Laboratory of Physical Chemistry,
Section of Materials Science and Engineering,
Department of Chemical Engineering,
National Technical University of Athens,
Iroon Polytechniou 9,
Zografou 157 80, Athens, Greece
E-mail: gpaterma@central.ntua.gr
Tel.: +30-1-7723203
Fax: +30-1-7723184

$(3.09\times10^{-6}\ cm^3\ mA^{-1}\ min^{-1})\cdot k_{d,a}$: $r_{d,a}a_{H+}{}^{-1}$ = average rate constant of the pore wall oxide dissolution · $k_{d,a,M}$: $r_{d,a,M}a_{H+}{}^{-1}$ = the maximum $k_{d,a}$ value obtained for the thickest film examined in each electrolyte · k_{eq}: equilibrium constant of the reaction Al^{3+}(bare sites) + $OH^-_{b/d} \rightleftharpoons Al^{3+}OH^-$ taking place in the barrier layer/double layer (b/d) interface · k_w: ionization constant of H_2O · κ: conductivity of solution · λ: $N_{1,m}\theta_{OH^-}{}^{-1}$ = constant · M^w: molar mass of Al_2O_3 · m: mass of oxide spread over the whole geometric surface area of Al specimens · m_F: mass of the Al consumed · m_{fi}: final (after anodization and drying) mass of the specimen · m_{in}: initial mass of the specimen · n: surface concentration of pores · N: Avogadro constant · $N_{1,m}$: surface concentration of the mobile OH^- ions · $N_{2,m}$: surface concentration of the mobile O^{2-} ions · v_1: vibration frequency of OH^-, or the number of chances per second the ions may jump the energy barrier if they have sufficient energy · v_2: vibration frequency of O^{2-}, or the number of chances per second the ions may jump the energy barrier if they have sufficient energy · n_1: valence of OH^- · n_2: valence of O^{2-} · p: porosity of the anodic film (volume/volume) · P_a: anodic potential · $P_{a,M}$: maximum value of the anodic potential achieved at a very low time, usually 6–7 s · $P_{a,m}$: minimum value of the anodic potential achieved at a low time, usually 2–3 min · $P_{a,c}$: limiting constant value of the anodic potential achieved on prolonged anodization · rc: reference anodization condition, C_{H2SO4} = 1.53 mol dm^{-3} and $C_{Al2(SO4)3} = 0$ · r_d: rate (length/time) of the pore wall oxide dissolution · $r_{d,a}$: average r_d value along the entire pore wall surface · $r_{d,a,M}$: the maximum $r_{d,a}$ value obtained for the thickest film examined in each electrolyte · R: universal gas constant · $R_{s,p}$: ohmic resistance of the solution inside the pores corresponding to the total geometric surface of the Al specimen · S_g: geometric surface area of Al specimens, 30.75 cm^2 · t: anodization time · t_l: time up to which the film thickness increases linearly with time · t_t: time at which the maximum pore diameter near or at the film surface approaches first the cell width · T: temperature · W_1: height of the energy barrier (activation energy) for the migration of OH^- ions · W_2: height of the energy barrier (activation energy) for the migration of O^{2-} ions.

Introduction

It is generally accepted that during the growth of porous anodic alumina films a steady state is established regarding both the thickness of the barrier layer and the formation and propagation of pores through the so-called "field assisted" oxide dissolution at pore bases [1, 2, 3, 4, 5, 6, 7, 8, 9]. The pores generally broaden towards the film surface as a result of the chemical dissolution of the oxide by the electrolyte present inside the pores [2, 3, 4, 5, 10], similar to the open circuit oxide dissolution process [3, 4, 5, 10, 11].

A large amount of work has been done on the porous structure [1, 2, 9, 12, 13, 14, 15, 16], porosity [17], nature/composition and incorporation of electrolyte anions [1, 2, 15, 18, 19], the mechanism and kinetics of growth [1, 2, 7, 20, 21, 22], properties [1, 2, 23, 24, 25, 26] and the scientific/technological applications of porous anodic aluminas in anticorrosion and decoration coatings of Al [1, 2, 24], magnetic memories of high bit density recording [26], membranes [27] and catalysis [28, 29, 30, 31, 32, 33, 34]. Also, work has been done on the growth of hard films [35, 36, 37, 38] and the appearance of phenomena related to non-uniform/nonregular oxide growth like pitting and burning [7, 22, 35, 39], both of which are favored by sulfate additives [7, 35, 36, 37, 38].

Nevertheless, the physicochemical processes in the barrier layer/electrolyte interface, inside this layer and in the metal/oxide interface and their mechanisms, which determine the whole mechanism of growth of porous films, still remain essentially unknown. This is valid also for the processes on the pore wall surface. The elucidation of the above mechanisms is of great importance. These mechanisms may explain the effects of different kinds and concentrations of anions and cations and therefore the effects of additives on the anodization process. The properties of a particular film formed in a given electrolyte may be predicted. Then, the design of films desired for a particular scientific and technological application will become possible. Methods of anodization may be devised in order to obtain normally grown films even in conditions where, otherwise, abnormally grown films would be obtained, etc.

In the present work, suitable kinetic studies were made on the growth of films in different sulfate electrolytes like pure H_2SO_4 mixtures of $H_2SO_4 + Al_2(SO_4)_3$ and $Al(HSO_4)_3$, $NaHSO_4$ and $KHSO_4$ solutions. Finally, by proper treatment of the derived kinetic parameters, new information was uncovered on the processes taking place inside the barrier layer/electrolyte interface, across this layer, inside the metal/oxide interface and at the pore wall surface, and their related mechanisms were deduced.

Experimental

Porous anodic Al_2O_3 films were prepared by the anodic oxidation of Al sheets, 0.5 mm thick and 99.5% pure. The Al metal composition, the shape and dimensions of both the Al anodes and Pb cathodes employed and the procedures for the wash, neutralization for electrolyte removal from pores, as well as the drying of Al specimens, have all been outlined in detail elsewhere [21]. The anodic oxidation was performed galvanostatically at 15 mA cm^{-2} at 25 °C in a thermostated and vigorously stirred bath solution of pure H_2SO_4 at concentrations of 15% (for which many data exist in the literature [1, 2, 8, 21, 22, 23, 40]), 25% and 45% w/v (or 1.53, 2.55 and 4.59 mol dm^{-3}, respectively). Anodic oxidation was also performed in solutions of $Al(HSO_4)_3$ at 1.53/3 = 0.51 mol dm^{-3} and $NaHSO_4$ and $KHSO_4$ at 1.53 mol dm^{-3}, which were prepared by mixing accordingly $Al_2(SO_4)_3$, NaOH and KOH with H_2SO_4 at suitable concentrations in order to examine the

effect of the species, mobility and charge of the electrolyte cation on the kinetics of film growth. The absolute ionic mobilities of the Al^{3+}, Na^+, K^+ and H^+ cations at 18 °C, for example, are 4.1×10^{-8}, 4.6×10^{-8}, 6.6×10^{-8} and 32.4×10^{-8} m s^{-1}/V m^{-1} [41], respectively; they increase in the same order. A mixture of H_2SO_4 (1.53 mol dm^{-3}) + $Al_2(SO_4)_3$ (0.34 mol dm^{-3}) solution was also employed in which the corresponding total SO_4^{2-} concentration (2.55 mol dm^{-3}) coincided with that in the 2.55 mol dm^{-3} H_2SO_4 solution.

Also a mixture H_2SO_4 (1.53 mol dm^{-3}) + $Al_2(SO_4)_3$ (0.77 mol dm^{-3}) solution was employed. As observed, this latter $Al_2(SO_4)_3$ concentration is a little higher than the saturation concentration of ~0.75 mol dm^{-3}. In this way the bath solution inside the pores was saturated (or nearly saturated), irrespective of some probable slight changes of temperature and composition of the anodizing solution inside the pores during the film growth. Also, the precipitate existing in small amounts in the bath could not exert any appreciable hindrance to the stirring of the solution. The specimens anodized in the $H_2SO_4 + Al_2(SO_4)_3$ (saturated) electrolyte were immersed in warm H_2O at ~35 °C for 5 min before their washing and neutralization via the standard procedure in order to remove any residual $Al_2(SO_4)_3$ precipitate from the pores. Hence, the mass of the film, which was determined as described below, was solely that of oxide.

Different as well as comparable concentrations of the H^+, SO_4^{2-}, HSO_4^- and Al^{3+} ions and identical, or almost identical, equivalent concentrations of the electrolyte cations are present in the electrolytes employed, for comparison purposes. The pH of all solutions was measured prior to their use with a suitable pH meter measuring at pH 0–14 with satisfactory accuracy and the H^+ ion activity was thus determined, 10^{-pH}. The quantity of the anodizing solution was large compared to the passing charge. Thus, the bulk pH and the H^+ activity would not change appreciably during anodization, as indeed verified. The pH of the most acidic H_2SO_4 solution, 4.59 mol dm^{-3}, was negative and the H^+ activity could not be deduced by this method. This particular H^+ activity was estimated from the H^+ activity in 2.55 mol dm^{-3} H_2SO_4 as 4.59/2.55 times the activity at 2.55 mol dm^{-3}, assuming that the activity coefficient does not vary appreciably with the H_2SO_4 concentration in this region of concentrations.

Since the pore/cell surface concentration depends solely on current density [7, 40], a constant current density was employed throughout the experiments to ensure a constant pore/cell surface concentration, thus facilitating appreciably the ensuing analysis. Different anodization times were employed to obtain average film thicknesses ranging between low values (tending to zero) and the maximum limiting ones attained on prolonged anodization; the maximum limiting or the approximate (quasi) maximum limiting thickness [1, 2, 21, 22] appears on prolonged anodization as a result of the general broadening of pores towards the film surface, owing to the pore wall oxide dissolution by the electrolyte inside the pores [2, 3, 4, 5, 10].

The anodic potential was determined using a suitable reference $Cu/CuSO_4$ (saturated) electrode, the pin mouth hole of which was attached to the vicinity of the Al specimen's lateral thin surface inside the bath solution. This electrode was chosen since it has a common anion with the bath solution and the passage of $CuSO_4$ in the solution in appreciable amounts could be checked by its coloration. Also, a negligible amount of Cu^{2+} probably passing into the bath cannot affect the process and measurements; it is easily and quickly discharged (deposited) on the Pb cathodes [42]. The anodic potential was followed during the entire anodization process and referenced to the hydrogen standard electrode potential, according to the usual practice for describing anodic or cathodic potentials.

The accurate masses of the films were determined as previously described [22] by the formula m_{fi}–m_{in}+m_F, which is based on mass balance, where m_{in}, m_{fi} and m_F are respectively the initial mass and the final (after anodization and drying) mass of the specimens and the mass of the Al consumed, which obeys Faraday's law [21, 22].

Results

Variation of the anodic potential with the anodization time; the potential drop across the hemispherical shell-shaped barrier layer in the steady state

The anodic potential (P_a) varies with the anodization time (t) at a current density (j) of 15 mA cm^{-2}, bath temperature (T) of 25 °C and the anodizing electrolytes employed, as shown in Fig. 1. Three successive stages are distinguished:

1. Within a short time interval, of the order of 1 s, usually 6–7 s, P_a increases abruptly up to a maximum value, $P_{a,M}$. During this stage a flat barrier-type oxide forms, the thickness of which increases linearly with t [7, 19, 20]. Pores appear at the end of this stage. $P_{a,M}$ is highest for the bisulfates and decreases abruptly with H_2SO_4 concentration (C_{H2SO4}) while only slightly with $Al_2(SO_4)_3$ concentration ($C_{Al2(SO4)3}$), mainly due to a similar variation in the thickness of the barrier layer. Secondary influences due to the oxide nature/composition, which varies across this layer [16, 19] and is affected by the conditions, cannot be excluded.
2. At the concomitant transient period of usually 2–3 min, P_a decreases and a minimum, $P_{a,m}$, appears; $P_{a,m}$ and $P_{a,M}$ vary with C_{H2SO4} and $C_{Al2(SO4)3}$ in a similar fashion. Early at this stage the pores and the barrier layer, in the form of a close-packed array of hemispherical shell units (Fig. 2), are completely formed; towards the end of this stage a steady state is established regarding the surface concentration and the base diameter of the pores, the barrier layer thickness and the oxide nature/composition across the layer. The latter may be affected by the thin oxide formed spontaneously on the Al surface before anodizing. Its nature/composition may act as a matrix for that of the barrier layer. Its influence decays with t and vanishes at $t \approx t(P_{a,m})$.
3. For $t > t(P_{a,m})$ a quasi-permanent state is observed. The nature/composition of the barrier layer is defined solely by the anodization conditions. P_a decreases slightly for the $NaHSO_4$ and $KHSO_4$ solutions while it increases slightly with t for the other solutions, more significantly so as C_{H2SO4} decreases and $C_{Al2(SO4)3}$ increases, until a limiting constant value, $P_{a,c}$, is established, or tends to be established, apparently when the average film thickness (h) becomes also the maximum limiting one (h_c). In contrast, at the highest $C_{Al2(SO4)3}$ employed and at high t values, P_a increases abruptly with t. It is apparent that for each electrolyte a strict steady state may be established only when $h = h_c$.

The growth of the initial flat barrier layer and its transformation to the close-packed array of hemispherical shell units is not examined here. This study deals with the (quasi) permanent state established at

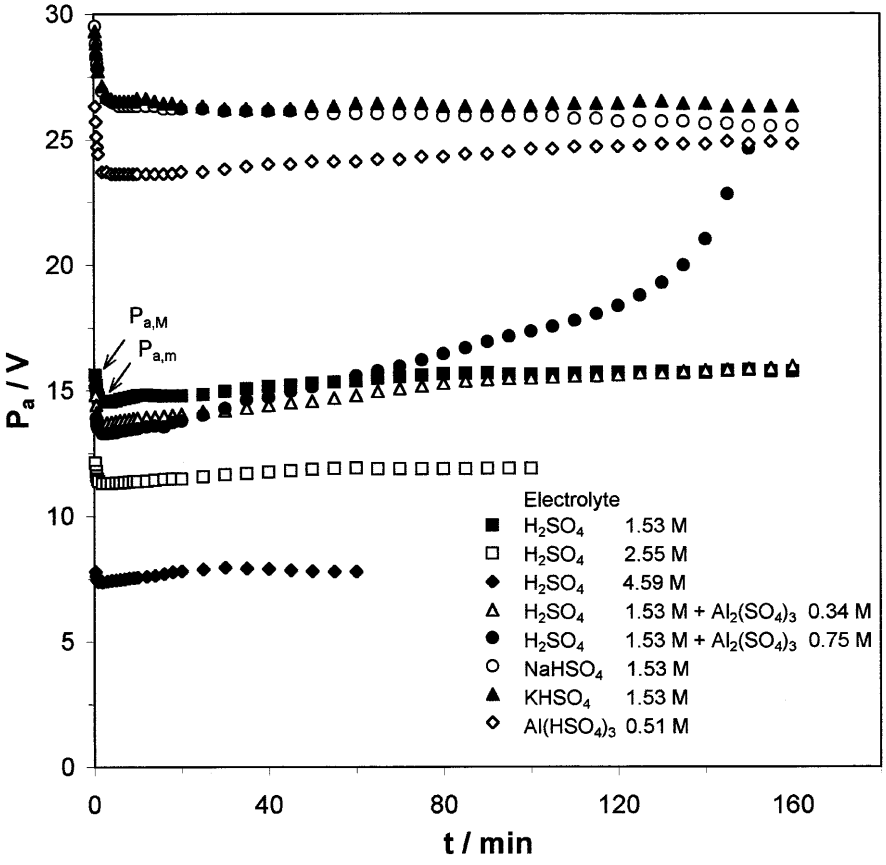

Fig. 1 Variation of the anodic potential with the anodization time at $T = 25$ °C and $j = 15$ mA cm^{-2} in different electrolytes

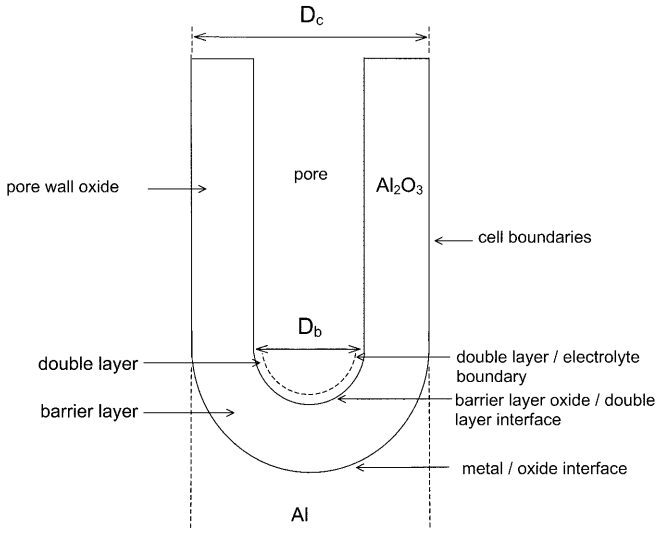

Fig. 2 Schematic representation of a section parallel to the pore axis of an elongated, columnar cell of a porous anodic alumina film. The pore, the pore base diameter D_b, the cell size D_c, the pore wall oxide, the hemispherical shell-shaped barrier layer, the metal/oxide interface, the cell boundaries, the double layer, the barrier layer/double layer interface and the double layer/pore filling electrolyte boundary during the film growth are all indicated

$t > t(P_{a,m})$, where influences of the thin oxide layer pre-existing on Al have been eliminated. For a satisfactory determination of the potential drop across the barrier layer, the potential drop across the porous layer must be assessed. As an example, this is estimated for an H_2SO_4 solution. Let ΔP_b, ΔP_p and ΔP_f be the respective potential drops across the barrier layer from the metal/oxide (m/o) interface up to the pore base oxide surface/double layer (b/d) interface, across the porous layer and across the entire film from the m/o interface up to the outer film surface/bath electrolyte interface. Then:

$$P_a \approx \delta P_f = \delta P_b + \delta P_p \quad (1)$$

It has been shown by a transport phenomenon analysis [43] that at low j values (e.g. $j \leq 25$ mA cm^{-2}), with $T = 25$ °C, $C_{H2SO4} = 1.53$ mol dm^{-3} and $h \leq 150$ μm, the concentration of $Al_2(SO_4)_3$ inside the pores is negligible in comparison to that of H_2SO_4; the conductivity inside the pores is determined almost exclusively by the H_2SO_4 concentration, which is variable along them. Also, the H_2SO_4 concentration does not vary significantly along the pores in comparison to the C_{H2SO4} value and can be considered as almost constant, i.e. 1.53 mol dm^{-3}. The above are also valid here for the H_2SO_4 electrolytes since j is low and $h << 150$ μm (see later).

The thickness of the barrier layer is generally very small, < 14 Å/V of imposed voltage [1, 2]. For not very thin films, as in the present case, the thickness of the barrier layer is always negligible in comparison to the total film thickness and, to a good approximation, the pore length equals the total film thickness. A

truncated cone pore shape can be roughly adopted [21, 22] and the average pore diameter (D) at a distance h from the pore base will be $D = D_b + (h/h_c)(D_c - D_b)$, where D_b and D_c are respectively the pore base diameter and the diameter at the pore mouths of an $h = h_c$ thickness film; in other words, the cell width (Fig. 2). The compact pore wall material is essentially an insulator with a thickness generally much higher than the barrier layer thickness, not allowing the passage of either an electronic or an ionic current. Therefore ΔP_p can be assessed only by the passage of current through the pore filling solution. The differential potential drop along the dh length of pores (dP_p) will be:

$$dP_p = j dR_{s,p} = jS_g\kappa^{-1}(4^{-1}\pi n S_g D^2)^{-1}dh$$
$$= j\kappa^{-1}(4^{-1}\pi n)^{-1}[D_b + (h/h_c)(D_c - D_b)]^{-2}dh \quad (2)$$

where $R_{s,p}$ is the ohmic resistance of the solution inside the pores corresponding to the total geometric surface area of the Al specimen ($S_g = 30.75$ cm^2 [21]), κ is the conductivity of solution, n is the surface concentration of the pores (pores/cm^2) and $4^{-1}\pi n S_g D^2$ is the total surface area occupied by the pores at a length h from the pore base.

The potential drop along the h length of pores from the pore base becomes:

$$\Delta P_{p,h} = \int_0^h j dR_{s,p}$$
$$= -j\kappa^{-1}\left(4^{-1}\pi n\right)^{-1}[(D_c - D_b)/h_c]^{-1}$$
$$\times\left\{[D_b + (h/h_c)(D_c - D_b)]^{-1} - D_b^{-1}\right\} \quad (3)$$

and for the maximum limiting thickness, h_c, it becomes:

$$\Delta P_{p,h_c} = j\kappa^{-1}\left(4^{-1}\pi n\right)^{-1}h_c(D_c - D_b)^{-1}\left(D_b^{-1} - D_c^{-1}\right)$$
$$= 4j\kappa^{-1}h_c\left(n^{1/2}D_c - n^{1/2}D_b\right)^{-1}$$
$$\times\left[\left(n^{1/2}D_b\right)^1 - \left(n^{1/2}D_c\right)^{-1}\right] \quad (4)$$

For each electrolyte the average film thickness is given from the equation:

$$h = k't = k''jt \ (t \le t_l) \quad (5)$$

where k' is the rate of the film thickness growth, k'' is a constant (3.09×10^{-6} cm^3 mA^{-1} min^{-1}) [21] and t_l is the time up to which the film thickness increases linearly with time [21]; t_l is generally slightly lower than or equal to the time t_t at which the pore diameter near or at the film surface approaches D_c and the film aspect starts to transform from being transparent and similar to the metal surface to a milky opaque one [21, 22]. The time t_t is close to the time at which the maximum limiting film thickness is first established, i.e. $h_c \approx k''jt_t$.

Equation 3 shows that $\Delta P_{p,h}$ increases with decreasing κ and increasing h; then, it becomes maximum for $h = h_c$. At $C_{H2SO4} = 1.53$ mol dm^{-3}, κ has an intermediate value among those of all the cases examined [41]; the same is valid for h_c as it is inferred from the corresponding t_t value (see below). For this reason the case where $C_{H2SO4} = 1.53$ mol dm^{-3} and $h = h_c$ is examined. At $C_{H2SO4} = 1.53$ mol dm^{-3}, $t_t = 110$ min (see below) and $h_c \approx k''jt_t = 51$ μm and $nD_b^2 = 0.327$, which was determined from the treatment of the film mass values by a suitable kinetic model (see later). Also, $nD_c^2 = 4/3$ [42]. From the κ value at $C_{H2SO4} = 1.53$ mol dm^{-3} and $T = 25$ °C [41], $\Delta P_{p,h_c} = 1.9$mV, i.e. negligible compared with P_a. Hence, irrespective of the real pore shape, ΔP_p is generally insignificant, i.e. $\Delta P_p \approx 0$ and $P_a \approx \Delta P_b$. In the ensuing analysis, $P_{a,m}$ is considered instead of $P_{a,c}$ (or P_a values at the maximum t values employed) since the $h(P_{a,m})$ values are low enough and both the variations of P_a, due to changes of electrolyte composition at the pore bases which generally increase with h [43], and ΔP_p are negligible.

Variation of the film mass with the anodization time; application of a suitable kinetic model and derivation of kinetic parameters

The film mass (m) spread over the whole geometric surface of the Al specimens varies with t for the electrolytes employed, as shown in Fig. 3; m increases with t with a decreasing rate and a maximum limiting value is (or tends to be) established on prolonged anodization. The approximate t_t values were ~110, ~75 and ~45 min for the pure 1.53, 2.55 and 4.59 mol dm^{-3} H_2SO_4 and ~110 and ~120 min for the H_2SO_4 (1.53 mol dm^{-3}) + $Al_2(SO_4)_3$ (0.34 mol dm^{-3}) and H_2SO_4 (1.53 mol dm^{-3}) + $Al_2(SO_4)_3$ (0.75 mol dm^{-3}) and ~200 min for the bisulfates. From Eq. 5 it is inferred that always $h < h_c < < 150$ μm, as previously noted.

Regular/uniform growth of porous anodic Al_2O_3 films occurs when pitting does not appear. When, in addition, any residual $Al_2(SO_4)_3$ precipitate does not remain in the pores after anodizing, then the following kinetic model applies for the stirred bath film growth [22]:

$$F = (kjt - m)(4^{-1}\pi S_g d_c k' t)^{-1} = F_0 + F_1 t + F_2 t^2$$
$$= 4^{-1}\pi p(F_0, F_1 \text{ and } F_2 > 0 \text{ and } t \le t_t) \quad (6)$$

where F is a dimensionless factor, k is a constant for oxide production resulting from Faraday's law, d_c is the density of the compact pore wall oxide (3.42 g cm^{-3}) [21], $F_0 = nD_b^2$, F_1 and F_2 are parameters depending on the conditions inside the pores and on the nature/composition and reactivity of the pore wall oxide and p is the film porosity (volume/volume).

The above relationship between F and p assigns a physical meaning to F. The F factor is useful to study the kinetics and mechanism of film growth since (1) it is directly related to important average structural features, like n, D_b, p, etc., and (2) it magnifies the m

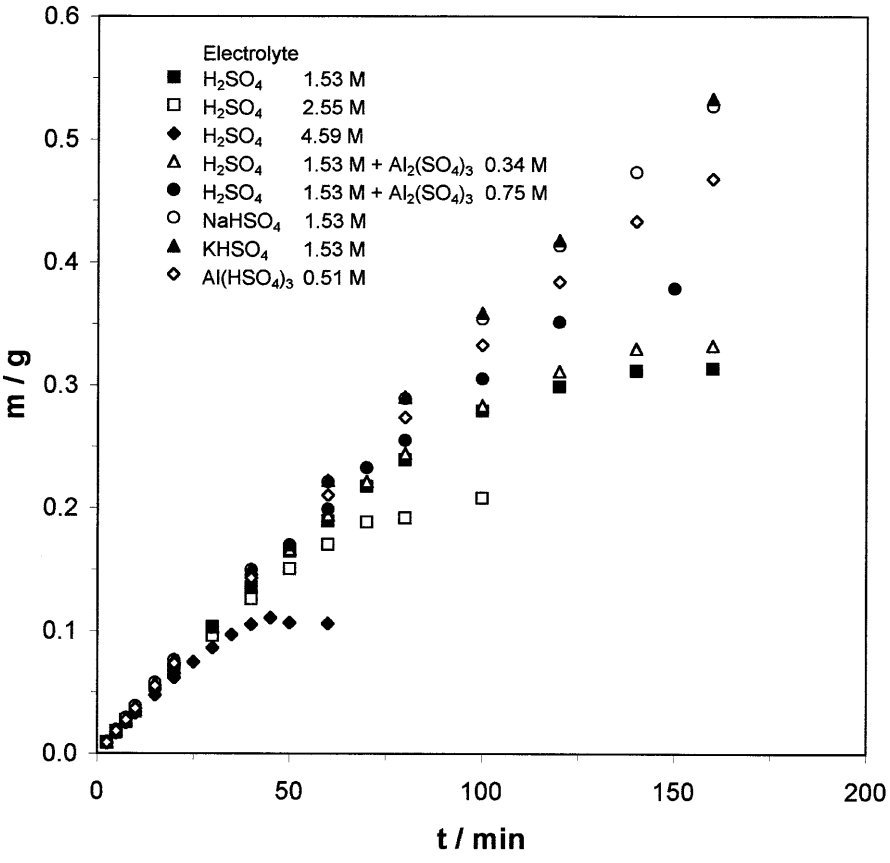

Fig. 3 Variation of the film mass spread over the 30.75 cm^2 geometric surface area of the Al specimens with the anodization time at $T = 25$ °C and $j = 15$ mA cm^{-2} in different electrolytes

differences, thus permitting a detailed and accurate analysis [22]. The F versus t plots are shown in Fig. 4. Equation 6 fits well the experimental points in all the cases, showing a regular oxide growth [22]. The derived F_0, F_1, F_2 and correlation coefficient (COR) values appear in Table 1.

Dependence of the pore base diameter on the H^+ activity

Since n depends exclusively on j [7, 40], the variation of nD_b^2 is attributed solely to the variation of D_b. The H^+ activities (a_{H+}) in the electrolytes employed appear in Table 1. It is inferred that nD_b^2 generally increases with a_{H+}. The $F_0^{-1} = (nD_b^2)^{-1}$ versus a_{H+}^{-1} plot is given in Fig. 5; a satisfactory straight line is observed with gradient 0.3947, intercept 2.2645 mol^{-1} dm^3 and COR = 0.9784. The effects of the electrolyte anions and cations per se are insignificant.

Dependence of the field strength across the barrier layer on the pore base diameter

Inside the barrier layer of porous anodic films the field strength is always very high, of the order of 10^7 V cm^{-1} [1, 2]. As shown in Fig. 2, the thickness of the barrier layer is $2^{-1}(D_c - D_b)$. The average field strength across this layer is $E_a = 2P_{a,m}(D_c - D_b)^{-1}$. From the values of $nD_c^2 = 4/3$ [42] and nD_b^2 (Table 1) and of n at the employed j, the real E_a values can be found. An inaccuracy in the E_a determination, however, might probably arise from the adoption of an n value from the ones found in the literature [7, 33]. In order to avoid such an inaccuracy, the relative field strength (E_r), i.e. the ratio of E_a at each condition to that of a condition considered as the reference condition (rc), e.g. $C_{H2SO4} = 1.53$ mol dm^{-3} and $C_{Al2(SO4)3} = 0$, was calculated from $P_{a,m}$ and the ratio $(n^{1/2}D_c - n^{1/2}D_b)/(n^{1/2}D_c - n^{1/2}D_b)_{(rc)}$. The E_r values are given in Table 1. The E_r versus $n^{1/2}D_b$ plot is shown in Fig. 6. The point for the $H_2SO_4 + Al_2(SO_4)_3$ (saturated) electrolyte deviates significantly upwards. It was excluded from the plot construction but it appears in Fig. 6 for comparison purposes. Two stepwise regions appear; the upper one is for the bisulfates.

The variation of the average rate constant of the pore wall oxide dissolution reaction across the pore walls; effect of the anodizing electrolyte on the rate constant

Since the j value employed and the h values obtained in this study are relatively low, it is expected that the composition of the pore filling solution does not vary

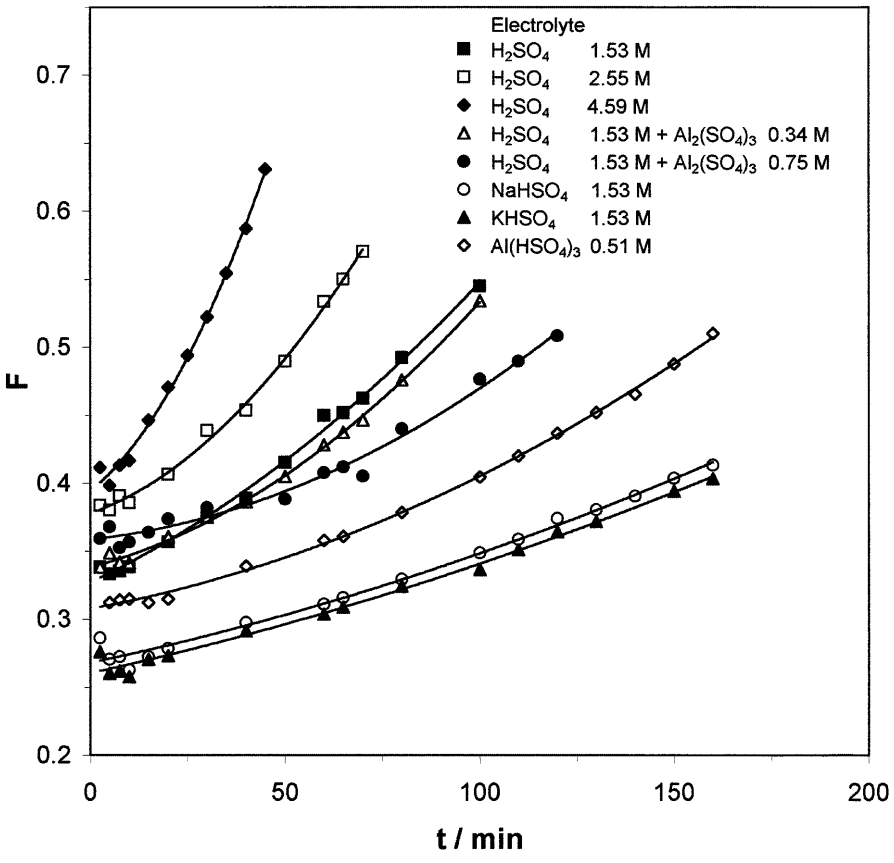

Fig. 4 Variation of the dimensionless factor F with the anodization time at $T = 25$ °C and $j = 15$ mA cm^{-2} in different electrolytes for $t \leq t_t$

Table 1 Values of the H^+ activity, a_{H+}, of the parameters F_0, F_1 and F_2 and correlation coefficient, COR, derived from the fitting of Eq. 6 to the experimental results, and of E_r in different electrolytes

Anodizing electrolyte	a_{H+} (mol dm^{-3})	$10^4 F_0$	$10^4 F_1$ (min^{-1})	$10^6 F_2$ (min^{-2})	COR	E_r
H_2SO_4 (1.53 mol dm^{-3})	0.52	3270	13.69	8.4	0.9978	1.00
H_2SO_4 (2.55 mol dm^{-3})	0.83	3778	10.18	25.1	0.9979	0.84
H_2SO_4 (4.59 mol dm^{-3})	1.50	3944	22.89	65.3	0.9976	0.56
H_2SO_4 (1.53 mol dm^{-3}) + $Al_2(SO_4)_3$ (0.34 mol dm^{-3})	0.62	3381	7.55	11.9	0.9986	0.95
H_2SO_4 (1.53 mol dm^{-3}) + $Al_2(SO_4)_3$ (0.75 mol dm^{-3})	0.74	3616	2.17	8.6	0.9835	0.96
$Al(HSO_4)_3$ (0.51 mol dm^{-3})	0.38	3078	5.24	4.5	0.9990	1.58
$NaHSO_4$ (1.53 mol dm^{-3})	0.25	2681	6.04	2.0	0.9923	1.66
$KHSO_4$ (1.53 mol dm^{-3})	0.28	2604	6.36	1.7	0.9926	1.65

essentially along the pores [43] and it is almost identical to that in the bulk solution for all electrolytes employed. When the composition of the electrolyte does not change significantly along the pores during film growth, as assumed here, and the rate of the pore wall oxide dissolution across the pore wall material remains constant, the average pore shape well approximates to that of a truncated cone. In this case the kinetic model $m = kjt - (12)^{-1}\pi n S_g d_c k' t(3D_b^2 + 6D_b r_d t + 4r_d^2 t^2)$ [21] is valid. It is easily transformed to the model (Eq. 6) in which $F_1 = 2nD_b r_d$ and $F_2 = (4/3)n{r_d}^2$, where r_d is the rate (length/time) of the pore wall oxide dissolution, which is a purely chemical process with an activation energy ~80 kJ mol^{-1} [21]. The $n^{1/2} r_d$ value can be calculated separately from these parameters, taking into consideration the $F_0 = nD_b{}^2$ values.

It was observed that the r_d values determined by F_2 were 1.81–14.08 times higher than those determined by F_1. Hence, the geometry of the pores deviates significantly from that of a truncated cone. This must be due mainly to the fact that r_d varies across the pore wall material. Because Eq. 6 does not permit the determination of the r_d value at each point on the pore wall surface for revealing its variation, the following methodology was conceived to test this suggestion. At each t or h, the approximate average r_d value, $r_{d,a}$, can be found from the F value, considering a truncated cone pore shape. Then $r_{d,a}$ must obey the equation:

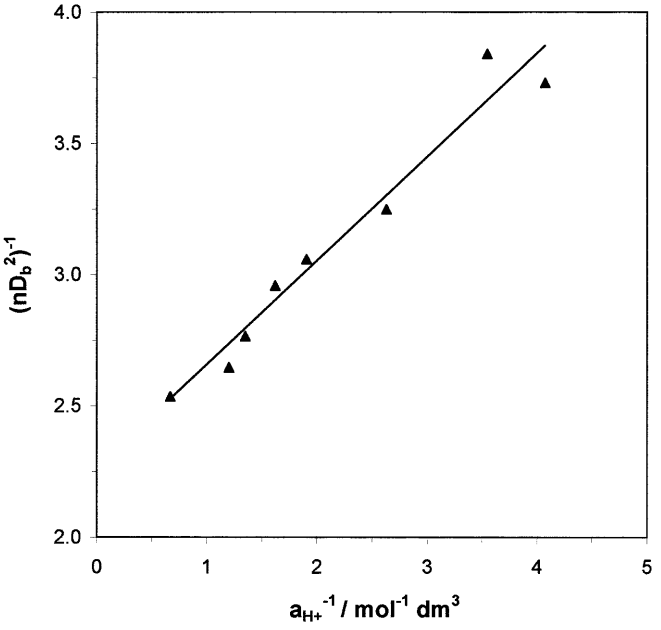

Fig. 5 Plot of $(nD_b^2)^{-1}$ versus a_{H+}^{-1}

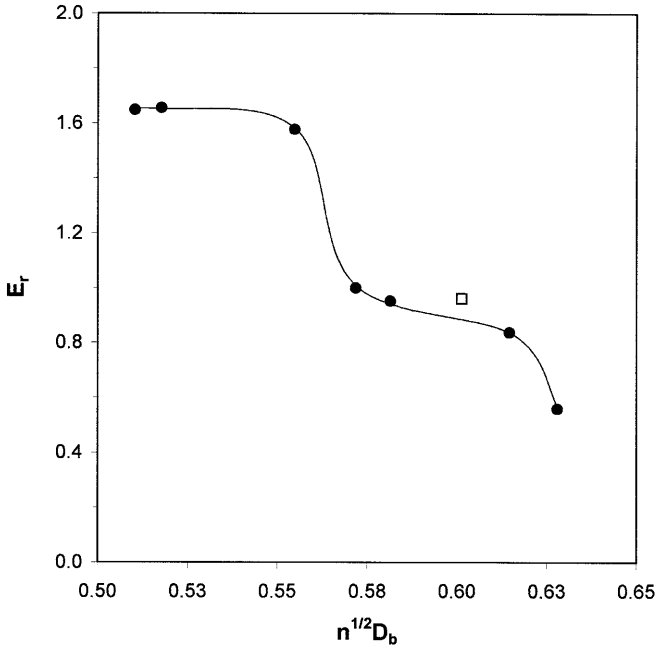

Fig. 6 Plot of E_r versus $n^{1/2}D_b$. The experimental point deviating significantly from the plot (*open square*) is for the electrolyte H_2SO_4 (1.53 mol dm^{-3}) + $Al_2(SO_4)_3$ (0.75 mol dm^{-3}) (saturated)

$$F = nD_b^2 + 2nD_b r_{d,a} t + (4/3) n r_{d,a}^2 t^2 \quad \text{or}$$

$$n^{1/2} r_{d,a} = \{-F_0^{1/2} + [(4/3)F - 3^{-1}F_0]^{1/2}\}[(4/3)t]^{-1} \quad (t \le t_t) \tag{7}$$

where $F_0 = nD_b^2$ is that found from the fitting of Eq. 6 to the experimental results.

There are two ways to work with Eq. 7 for each electrolyte. The first way is to introduce the experimental F values into this equation and calculate the corresponding separate $n^{1/2}r_{d,a}$ values. Because an appreciable scatter of the experimental results appears in the F versus t plots when $t \to 0$ (Fig. 4), the experimental F values may be lower than F_0 and negative $r_{d,a}$ values may be found at low t values without a physical meaning. An alternative way is to introduce second-order polynomial equations, fitting satisfactorily the results into Eq. 7 and derive the $n^{1/2}r_{d,a}$ values as a function of F_0 and t. In this case, negative $r_{d,a}$ values cannot be obtained and the tracing of the relevant $r_{d,a}$ versus t plots is easier. For these reasons the second option was chosen. The $r_{d,a}$ versus t plots are shown in Fig. 7. Generally, $r_{d,a}$ increases with t (or h) or it increases across the pore walls. The most representative $r_{d,a}$ values along the whole cross section of the pore walls are the maximum ones, i.e. those at t_t values or at the highest t values employed, $r_{d,a,M}$.

As previously noted, the average a_{H+} inside the pore filling solution does not differ appreciably from that in the bulk solution [43]. The $n^{1/2}r_{d,a,M}$ versus a_{H+} plot is given in Fig. 8. The plot was constructed excluding the experimental point concerning the $H_2SO_4 + Al_2(SO_4)_3$ (saturated) solution, which deviates strongly downwards and appears in Fig. 8 for comparison purposes. A satisfactory straight line is observed with gradient 2.23 min^{-1} mol^{-1} dm^3, intercept 2×10^{-4} min^{-1} (close to 0) and COR = 0.991. Hence:

$$n^{1/2} r_{d,a,M} = n^{1/2} k_{d,a,M} a_{H+} \tag{8}$$

where $n^{1/2}k_{d,a,M} \approx 2.23$ cm^3 min^{-1} mol^{-1}. Adopting that $n = 1.269\times10^{11}$ cm^{-2} at $j = 15$ mA cm^{-2} [33], then $k_{d,a,M} \approx 6.3\times10^{-6}$ cm^4 min^{-1} mol^{-1}, which agrees well with earlier results [3, 5, 10, 11, 21]. The main species in the pore filling solution directly involved in the slow step of the entire process is H^+. The pore wall dissolution is a first-order reaction as regards a_{H+}. The effects of the electrolyte anions and metal cations per se seem to be insignificant.

Plots of the average rate constant $n^{1/2}k_{d,a} = n^{1/2}r_{d,a}a_{H+}^{-1}$ versus t were constructed (Fig. 9). The $n^{1/2}k_{d,a}$ value always increases with t (or h) or across the pore walls from the pore wall surface towards the cell boundaries. The relative positions of the $n^{1/2}k_{d,a}$ versus h/h_c (reduced thickness) plots are shown in Fig. 10. These were constructed considering that $h_c \approx k'' j t_t$, or $h/h_c \approx t/t_t$, which is approximately valid [21, 22]. The plots in Figs. 7, 9 and 10 were traced by fitting second-order polynomials. At each h or h/h_c, $n^{1/2}k_{d,a}$ depends on the electrolyte.

Discussion

The processes in the pore wall surface/electrolyte and pore base surface/double layer interfaces

The surface of γ-Al_2O_3 in aqueous solutions takes up H_2O and is quickly hydroxylated:

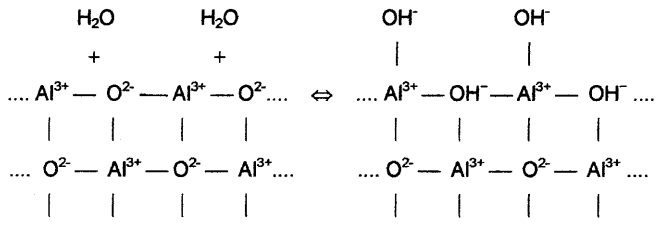

(9)

Also γ-Al_2O_3, among other mineral oxides in suspension in aqueous solutions, tends to be electrically charged and the isoelectric point (IEP) is at pH≈8. In acidic medium, pH < 8, the surface of alumina particles is positively charged and surrounded by anions, whereas at pH > 8 the inverse situation occurs [44, 45] according to the equations:

$$Al^{3+} - OH^- + H^+, A^- \leftrightharpoons Al^{3+} - OH_2^+, A^- \quad (10)$$

$$Al^{3+} - OH^- + B^+, OH^- \leftrightharpoons Al^{3+} - O^{2-}, B^+ + H_2O \quad (11)$$

where A^- and B^+ are the anions and cations. Both processes occur simultaneously but the first predominates in acidic and the second in basic media. This is also valid in the case of anodic alumina, which is an active microcrystalline material [46], although the IEP may differ.

Nevertheless, at the b/d interface the above processes change considerably under the action of high field strength. The decomposition of H_2O and the addition of OH^- on surface Al^{3+} are reinforced while the simultaneously produced H^+ are strongly pushed and removed away from the interface. The pH in the double layer becomes higher than in the pore filling solution and decreases from the b/d interface towards the boundary between the double layer and the solution. Hence, OH^- are added on surface Al^{3+} sites, H^+ are not added on surface O^{2-} sites and the positive surface charging (Eq. 10) is prevented.

The adsorption of OH^- on Al^{3+} weakens the bonding between these Al^{3+} and the neighboring lattice and surface O^{2-}. The surface O^{2-} are easily removed by the field from their initial positions towards the m/o interface, leaving voids. The removal of surface O^{2-} and the weakening of the bonding around the Al^{3+} favor simultaneously the removal of OH^- from the Al^{3+} sites and their re-adsorption on these anion voids, which thus act as active paths, the migration of OH^- towards the m/o interface and the solvation of Al^{3+}. The addition of OH^- on Al^{3+} and its migration towards the m/o interface may occur more than once between the time of emergence of an Al^{3+} on the surface from the innermost layers and its rejection in the pore filling solution. A distribution of the residence time of OH^- on Al^{3+} may well exist. New Al^{3+} and O^{2-} from the oxide lattice emerge on the surface, then the above processes repeat, etc.

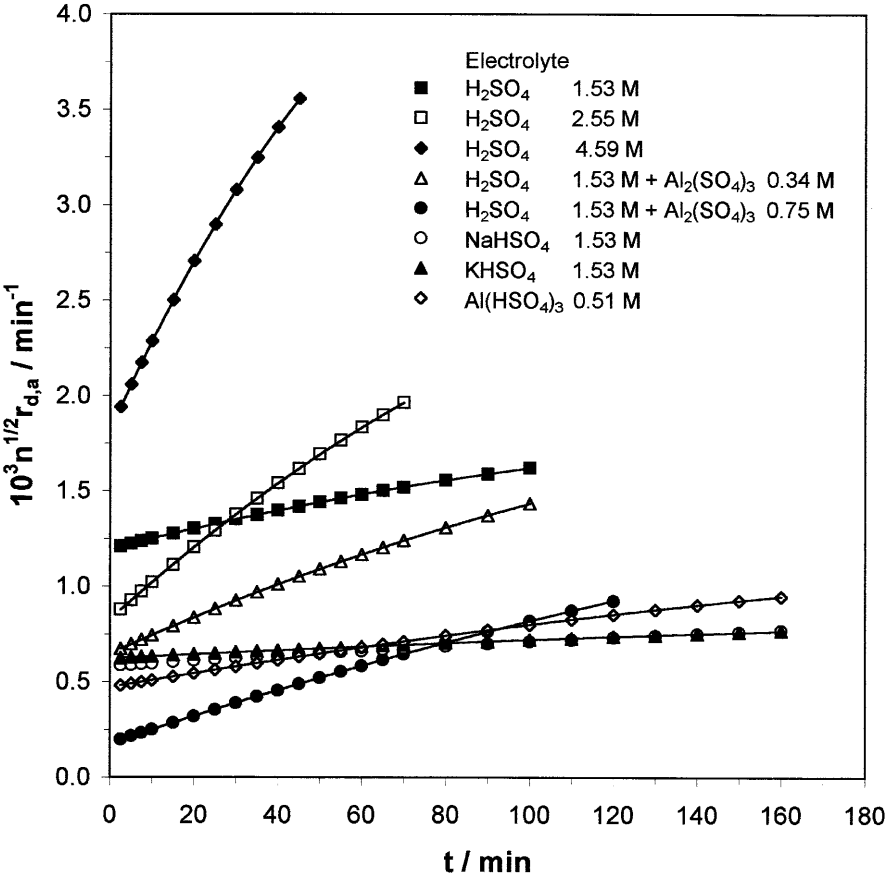

Fig. 7 Plots of $n^{1/2}r_{d,a}$ versus anodization time at $T = 25$ °C and $j = 15$ mA cm^{-2} in different electrolytes

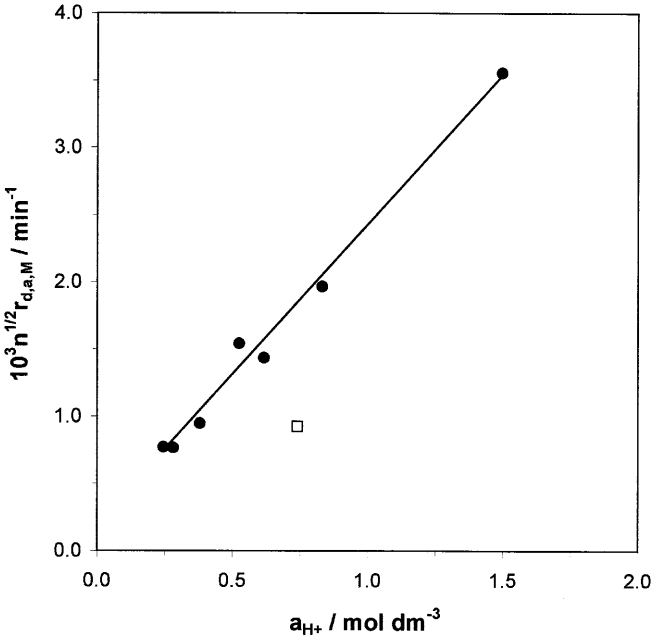

Fig. 8 Plot of $n^{1/2}r_{d,a,M}$ versus a_{H+}. The experimental point deviating strongly from the plot (*open square*) is for the electrolyte H_2SO_4 (1.53 mol dm^{-3}) + $Al_2(SO_4)_3$ (0.75 mol dm^{-3}) (saturated)

From the above it is evident that the equilibrium process which almost exclusively takes place on the pore base surface is the hydroxylation of surface Al^{3+} sites:

$$Al^{3+}(\text{bare sites}) + H_2O_{b/d} \rightleftharpoons Al^{3+}OH^- + H^+_{b/d} \qquad (12)$$

where the index b/d means the corresponding interface. Taking into consideration the equilibrium dissociation reaction of H_2O at the interface:

$$H_2O_{b/d} \rightleftharpoons OH^-_{b/d} + H^+_{b/d} \qquad (13)$$

Eq. 12 then becomes:

$$Al^{3+}(\text{bare sites}) + OH^-_{b/d} \rightleftharpoons Al^{3+}OH^- \qquad (14)$$

Hence, in the steady state, the pore base surface consists of the species Al^{3+}, O^{2-} and OH^-, with corresponding surface coverage fractions $\theta_{Al3+,b}$, θ_{O2-} and θ_{OH-}, for which:

$$\theta_{Al3+,b} + \theta_{OH-} = \theta_{Al3+} = 1 - \theta_{O2-} \qquad (15)$$

where $\theta_{Al3+,b}$ and θ_{Al3+} are correspondingly the fractions of the bare Al^{3+} not occupied by OH^- and of all the Al^{3+} sites. Since the ratio of the Al^{3+} and O^{2-} in the bulk of Al_2O_3, and therefore on its surface when OH^- are not adsorbed, is constant, then θ_{O2-} and θ_{Al3+} are

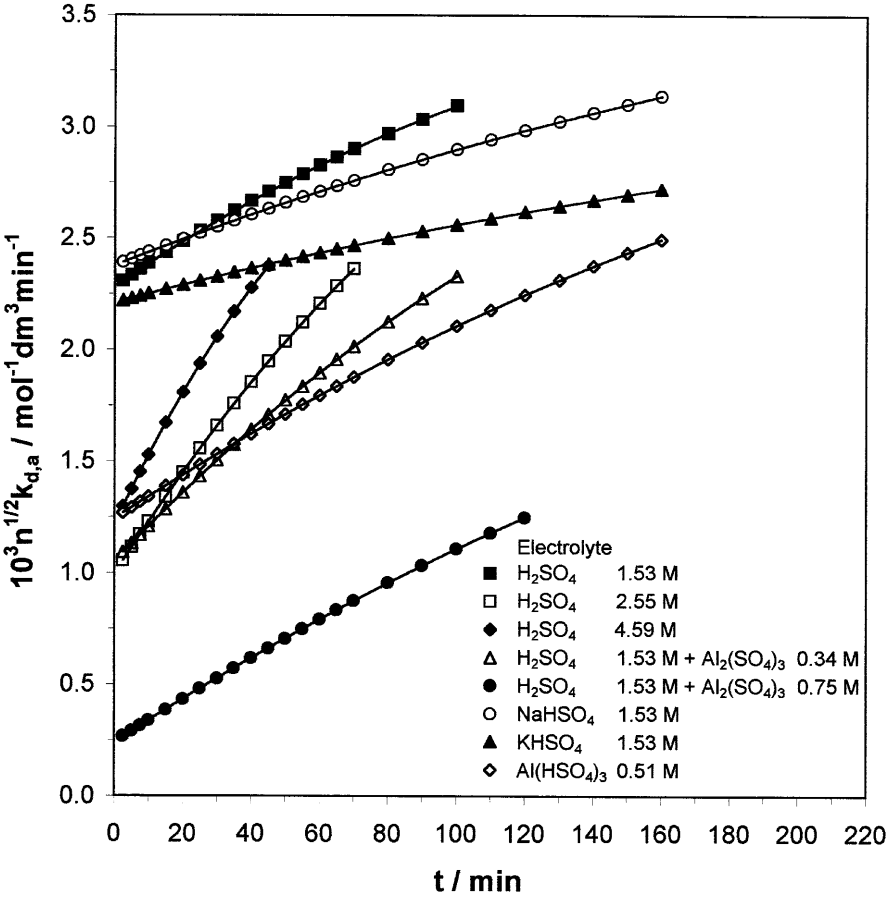

Fig. 9 Plots of $n^{1/2}k_{d,a}$ versus anodization time at $T = 25$ °C and $j = 15$ mA cm^{-2} in different electrolytes

also constant. A portion of $\theta_{Al3+,b}$ is covered by electrolyte anions. These are large and the solvated ones, being much larger and not mobile enough, are relatively weakly adsorbed. The small size and high mobility of OH^- favor their strong adsorption on Al^{3+}. From Eq. 14:

$$k_{eq} = \theta_{OH-}(\theta_{Al3+} - \theta_{OH-})^{-1} a_{OH-,b/d}^{-1} \text{ or}$$
$$\theta_{OH-} = k_{eq}\theta_{Al3+} a_{OH-,b/d}(k_{eq} a_{OH-,b/d} + 1)^{-1} \quad (16)$$

where $a_{OH-,b/d}$ is the OH^- activity at the interface and k_{eq} is the equilibrium constant. Because the OH^- concentration ($C_{OH-,b/d}$) is low enough, then, to a good approximation, $a_{OH-,b/d} = C_{OH-,b/d}$.

The mechanism of the charge transport processes inside the barrier layer

The enthalpy of HSO_4^- formation in aqueous solutions is low, $\Delta H° = -892.4$ kJ mol^{-1} [41]. It is close to, but higher than, that of SO_4^{2-}, –903.7 kJ mol^{-1} [41]. Hence, HSO_4^- is unstable in relation to SO_4^{2-} and decomposes easily according to $HSO_4^- \rightarrow H^+ + SO_4^{2-}$ inside the double layer, as a result of a pH increase inside it and of high field strength. At any rate, electrolyte anions incorporated in the barrier layer are almost exclusively SO_4^{2-} ions (see later). Owing to their very low formation enthalpy and their symmetry, these ions are stable and do not further decompose, yielding for example O^{2-}, even under such high field strengths like those developed across the barrier layer. Previously [42], it was found that the valencies of the anions migrating across the barrier layer are –1 and –2. Inside the bulk of the compact microcrystallites constituting the barrier layer [15, 46, 47] the migrating anions can only be O^{2-} and OH^- and not the electrolyte anions. The latter are much larger and cannot penetrate into the microcrystallites; instead, they can pass through intercrystalline spaces.

Electrolyte anions per se do not contribute to the Al oxidation; for this reason the mechanism of their incorporation and their indirect participation, to some small extent, in the Al oxidation process will be discussed later. The necessary O^{2-} for the Al oxidation comes from the oxide lattice O^{2-} and the OH^- adsorbed on the pore base surface.

During the growth of porous anodic alumina films, Al is consumed according to Faraday's law [21]. Oxide forms exclusively in the m/o interface according to Faraday's law [42, 48] at a rate (mol/time) equal to

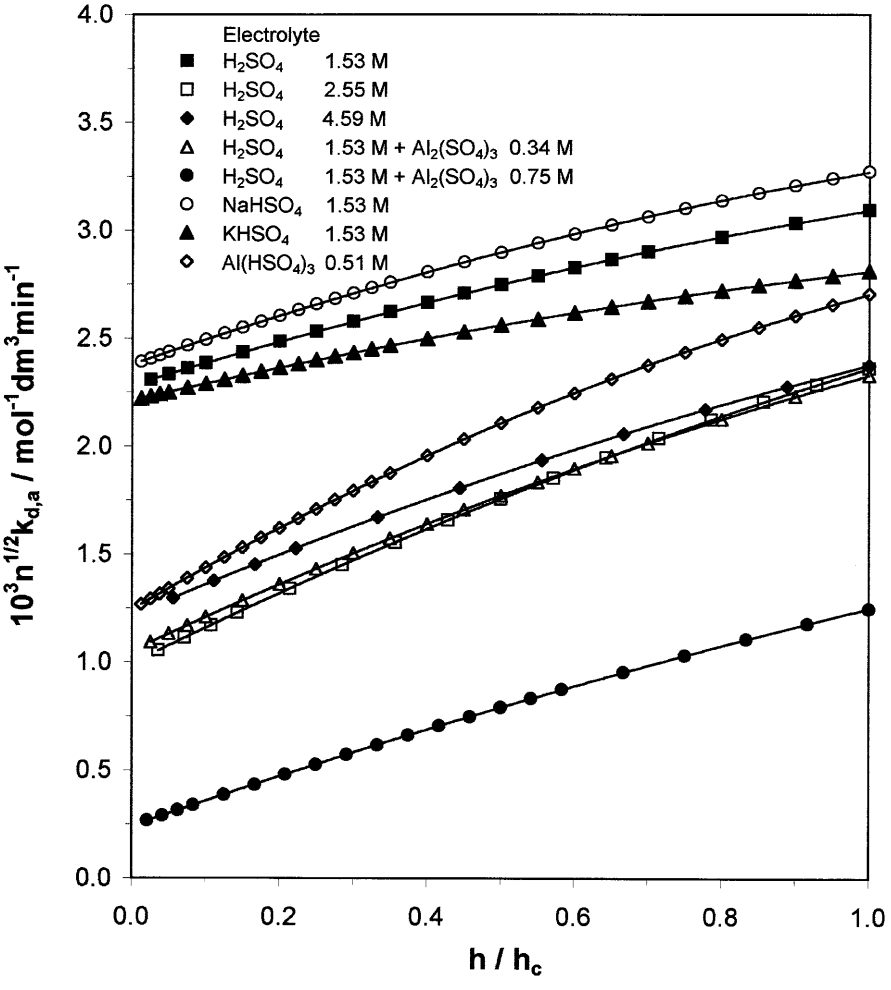

Fig. 10 Plots of $n^{1/2}k_{d,a}$ versus h/h_c at $T = 25$ °C and $j = 15$ mA cm^{-2} in different electrolytes

$jS_g(6F_c)^{-1} = 4^{-1}M_w^{-1}S_g\pi k'' jd_c nD_c^2$ or, since $\pi nD_c{}^2 \approx 4$, $\sim M_w{}^{-1}S_g k'' jd_c$, where F_c is Faraday's constant and M_w is the molar mass of Al_2O_3. The Al^{3+} are immobile inside the barrier layer [42]. Hence, the amount of O^{2-} required for Al oxidation reaches the interface at a rate obeying Faraday's law, $3jS_g(6F_c)^{-1} = (3/4)M_w^{-1}$ $S_g\pi k'' jd_c nD_c^2 \approx 3M_w^{-1}S_g k'' jd_c$. The net rate of oxide production is $4^{-1}M_w^{-1}S_g\pi k'' jd_c n(D_c^2 - D_b^2) = 4^{-1}M_w^{-1}S_g\pi$ $k'' jd_c nD_c^2(1 - D_b^2D_c^{-2}) = jS_g(6F_c)^{-1}(1 - D_b^2D_c^{-2}) \approx M_w^{-1}$ $S_g k'' jd_c(1 - D_b^2D_c^{-2})$. The rate of the supposed pore base surface oxide dissolution, defined by the shift of that surface towards the m/o interface, is $4^{-1}M_w^{-1}S_g\pi k'' jd_c n$ $D_b^2 = jS_g(6F_c)^{-1}D_b^2D_c^{-2} \approx M_w^{-1}S_g k'' jd_c\ D_b^2D_c^{-2}$. The rate of Al^{3+} rejection in the pore base solution is $2^{-1}M_w^{-1}S_g\pi k'' jd_c nD_b^2 = 2jS_g(6F_c)^{-1}D_b^2D_c^{-2} \approx 2M_w^{-1}\ \ S_g k''$ $jd_c D_b^2D_c^{-2}$.

The migration of O^{2-} and OH^- inside the barrier layer at comparable rates is possible since the ionic radius of O^{2-}, 1.32 Å [49], is higher than that of OH^-, ~0.96 Å [50], while the charge of O^{2-} is higher than that of OH^-. The enthalpy of OH^- formation is not low enough, e.g. in aqueous solution $\Delta H° = -229.7$ kJ mol^{-1} [41]. The OH^- can gradually decompose under the high field strength while moving inside the barrier layer. The product O^{2-} migrate towards the Al side while the H^+ migrate towards the b/d interface and are finally rejected [42].

In the steady state the O^{2-} coming from the pore base surface migrate to and reach the m/o interface at a rate J_{O2-}:

$$J_{O2-} = 3jS_g(6F_c)^{-1}D_b^2D_c^{-2} \tag{17}$$

The necessary additional O^{2-} reach the m/o interface at a rate $3jS_g(6F_c)^{-1}(1-D_b{}^2D_c{}^{-2})$. These O^{2-} come from the OH^- ions which leave the pore base surface at a rate J_{OH-}, which equals the above. The rate of H^+ rejection in the pore filling solution, J_{H+}, equals J_{OH-}. The total rate of charge transport through that surface (which equals that across the barrier layer) is jS_g or:

$$2J_{O_{2-}} + J_{OH-} + J_{H+} = 2J_{O_{2-}} + 2J_{OH-} = jS_gF_c^{-1} \tag{18}$$

The Al^{3+} transport number is zero, exactly as that across the barrier layer [42]. Hence:

$$J_{OH-} = 2^{-1}jS_gF_c^{-1} - 3jS_g(6F_c)^{-1}D_b^2D_c^{-2} \tag{19}$$

The shift of the pore base surface to the m/o interface is an electrochemical process as regards the migrations of the O^{2-} and OH^- ions, but the rejection of Al^{3+} in the pore filling solution is an ion solvation process. The latter, nevertheless, is field assisted by the migration of neighboring anionic species and the weakening of the bonding of Al^{3+} with these species. The validity of the suggested processes and mechanisms must be tested. Their ability to satisfactorily explain the variation of both D_b with a_{H+} and E_r with D_b is the best proof.

Interpretation of the variations of D_b with a_{H+} and of E_a (or E_r) with D_b

The true ionic current densities of OH^- and O^{2-} leaving the pore base surface are $j_{OH-,t} = j_{OH-} - S_g^{-1}(2^{-1}\pi nD_b^2)^{-1}$ and $j_{O_{2-}}, t = 2J_{O_{2-}}S_g^{-1}(2^{-1}\pi nD_b^2)^{-1}$. From Eqs. 17 and 19:

$$\begin{aligned} j_{OH-,t} &= j_{OH-} - S_g^{-1}(2^{-1}\pi nD_b^2)^{-1} \\ &= [2^{-1}jS_gF_c^{-1} - 3jS_g(6F_c)^{-1}D_b^2D_c^{-2}]S_g^{-1}(2^{-1}\pi nD_b^2)^{-1} \\ &= jF_c^{-1}(\pi nD_b^2)^{-1} - jF_c^{-1}(\pi nD_c^2)^{-1} \\ &= jF_c^{-1}(\pi nD_b^2)^{-1} - (3/4)jF_c^{-1}\pi^{-1} \end{aligned} \tag{20}$$

$$\begin{aligned} j_{O_{2-}},t &= 2J_{O_{2-}}S_g^{-1}(2^{-1}\pi nD_b^2)^{-1} \\ &= 2[3jS_g(6F_c)^{-1}D_b^2D_c^{-2}]S_g^{-1}(2^{-1}\pi nD_b^2)^{-1} \\ &= 2jF_c^{-1}(\pi nD_c^2)^{-1} = (3/2)jF_c^{-1}\pi^{-1} \end{aligned} \tag{21}$$

These ionic current densities should obey the high-field Cabrera-Mott equation [51]:

$$\begin{aligned} &jF_c^{-1}(\pi nD_b^2)^{-1} - (3/4)jF_c^{-1}\pi^{-1} \\ &\quad = N_{1,m}v_1n_1F_cN^{-1}\exp[(-W_1N + n_1a_1F_cE_b)/RT] \\ &\quad = \lambda\theta_{OH-}v_1n_1F_cN^{-1} \\ &\qquad \times \exp[(-W_1N + n_1a_1F_cE_b)/RT] \end{aligned} \tag{22}$$

$$\begin{aligned} &(3/2)jF_c^{-1}\pi^{-1} \\ &\quad = N_{2,m}v_2n_2F_cN^{-1}\exp[(-W_2N + n_2a_2F_cE_b)/RT] \end{aligned} \tag{23}$$

where $N_{1,m}$ is the surface concentration of the mobile OH^- which is proportional to θ_{OH-}, $N_{1,m} = \lambda\theta_{OH-}$, $N_{2,m}$ is the surface concentration of the mobile O^{2-} which is proportional to θ_{O2-} and constant, v_1 and v_2 are the ion vibration frequencies, i.e. the number of chances per second the ions may jump the energy barriers if they possess sufficient energies, W_1 and W_2 are the heights of these barriers, i.e. the activation energies, n_1 and n_2 are the ions valences, a_1 and a_2 are the activation (half-jump) distances, N is the Avogadro constant, R is the universal gas constant, T is the temperature in K and E_b is the field strength on the surface.

Equation 23 shows that, for constant T, E_b depends solely on j. Since j was kept constant, E_b is also constant. Then, θ_{OH-} and D_b are the variables in Eq. 22, which shows that when θ_{OH-} decreases, D_b necessarily increases. The latter equation becomes:

$$\begin{aligned} (nD_b^2)^{-1} &= 3/2 + j^{-1}\pi F_c\,\lambda\,\theta_{OH-}v_1n_1F_cN^{-1} \\ &\qquad \times \exp[(-W_1N + n_1a_1F_cE_b)/RT] \end{aligned} \tag{24}$$

For the electrolyte solution, $a_{H+}a_{OH-} = k_w$, where a_{OH-} is the OH^- activity (or, as previously noted, the OH^-

concentration) and k_w is the H_2O ionization constant. This a_{OH^-} is almost identical to that beyond the double layer. The field strength in the double layer/pore filling solution boundary is $(4^{-1}\pi n D_b^2)^{-1} j\kappa^{-1}$ [43]. This field strength is calculated for the case $C_{H2SO4} =$ 1.53 mol dm^{-3} and $T = 25$ °C, where it is expected to have an intermediate value. From the values of κ [41] and nD_b^2 (Table 1), this is found to be 0.106 V cm^{-1}, i.e. negligible compared to E_a, and can be considered almost independent of the electrolyte.

It is reasonable to accept that $a_{OH-,b/d} = a_{OH-} + b$, where b is the increase of the OH^- activity (or concentration) in the double layer. It is almost constant since the difference between the field strength on the pore base surface and that beyond the double layer is essentially always constant. The activity (or concentration) of H^+ in the interface decreases. The value of k_{eq} may depend on E_b. Since E_b is constant, k_{eq} is also constant. The electrolytes are strongly acidic and therefore $a_{OH^-,b/d}$ and θ_{OH^-} are small enough and $\theta_{OH^-} \ll \theta_{Al3+}$ or $\theta_{OH^-}(\theta_{Al3+} - \theta_{OH^-})^{-1} \ll 1$. From Eq. 16, $\theta_{OH^-}(\theta_{Al3+} - \theta_{OH^-})^{-1} = k_{eq} a_{OH^-,b/d} \ll 1$ and Eq. 24 becomes:

$$(nD_b^2)^{-1} \approx 3/2 + \{j^{-1}\pi F_c \lambda v_1 n_1 F_c N^{-1} \times \exp[(-W_1 N + n_1 a_1 F_c E_b)/RT]\} \times k_{eq}\theta_{Al_{3+}}(k_w a_{H^+}{}^{-1} + b) \quad (25)$$

Hence, $(nD_b^2)^{-1}$ is a linear function of $a_{H^+}{}^{-1}$, consistent with Fig. 5.

The decomposition of OH^- and the migration of the product H^+ inside the barrier layer requires a field strength higher than that on the pore base surface. This is probably due to the tendency of H^+ to recombine with O^{2-} in thermodynamically advantageous sites, e.g. in low-adsorption enthalpy sites. This tendency is reinforced towards the m/o interface, owing to a concomitant increase of the local bulk O^{2-} concentration, while the local field strength similarly increases. As the total rate of OH^- decomposition across the barrier layer increases, or as the rate of OH^- migration from the pore base surface increases, or, from Eq. 19, as D_b decreases, E_a increases, in agreement with Fig. 6.

For high D_b values, i.e. $n^{1/2}D_b \geq \sim 0.575$, or, from Eqs. 17 and 19, for $J_{OH^-}/J_{O2^-} < \sim 3.03$, almost all OH^- must have decomposed prior to reaching the m/o interface. For $n^{1/2}D_b < \sim 0.575$, or for $J_{OH^-}/J_{O2^-} > 3.03$, OH^- at a valuable rate reach the interface where their decomposition needs a local potential drop and field strength much higher than those inside the barrier layer. Then, E_a increases abruptly with the above rate or with decreasing D_b.

This abrupt rise of the potential drop in the m/o interface must be due to the formation of hydrates, instead of dry oxide, the decomposition of which needs a field strength much higher than that of the OH^- decomposition inside the barrier layer. This strong increase of E_a occurs up to $n^{1/2}D_b \approx 0.55$ or $J_{OH^-}/J_{O2^-} \approx 3.41$. For $n^{1/2}D_b \leq \sim 0.55$, E_a is high enough and the rate of OH^- reaching the interface acquires a maximum limiting value. Then, as D_b decreases, or J_{OH^-} increases, the rate of OH^- decomposition inside the barrier layer increases, causing a slight rise of E_a. The full elucidation of the latter phenomena needs further investigation.

The mechanism of the pore wall oxide dissolution

The surface is quickly hydroxylated (Eq. 9). Owing to the low pH values and the absence of an electrical field, the predominant process charging the surface is Eq. 10 [44, 45]; H^+ ions react with the surface OH^-, producing H_2O adsorbed on Al^{3+} sites. This is the slow step of the whole process. Anions HSO_4^- and/or SO_4^{2-} are also adsorbed. When oxide dissolves, i.e. at low pH values as here, the Al^{3+} are solvated and rejected in the solution; this process is assisted by the adsorbed H_2O and anions. The total equivalent reaction is $Al_2O_3 + 3H_2SO_4 \rightarrow 3H_2O + Al_2(SO_4)_3$. This mechanism is consistent with the results.

Interpretation of the variation of the rate constant of the pore wall oxide dissolution across the pore walls and with the kind and concentration of the anodizing electrolyte

In the following analysis, when necessary the approximate concentrations of SO_4^{2-} and HSO_4^- may be estimated by taking into consideration that the first dissociation of H_2SO_4 is complete while the second one is incomplete with a dissociation constant of $\sim 1.2 \times 10^{-2}$ [41].

Always small amounts of H_2O (either as H_2O molecules or as OH^- and H^+ ions) [21, 46] and considerable amounts of electrolyte anions [15, 19] are incorporated in the barrier layer. Their local concentrations vary across this layer. The local average size of the microcrystallites constituting the barrier layer [15, 46, 47] increases from the pore base surface towards the m/o interface [15]. The variations of the above concentrations and of the crystallite sizes across this layer are extrapolated on the pore wall surface of an h_c thickness film [52].

The pore wall dissolution must be retarded by the incorporated electrolyte anions. Their effect seems to be more significant than that of the other inclusions and crystallite sizes across the pore walls. The monotonic increase of $n^{1/2}k_{d,a}$ towards the cell boundaries denotes that the electrolyte anions concentration decreases monotonically across the barrier layer.

Their average concentration across the barrier layer must depend primarily on their concentration in the pore base solution. Secondary effects may be also exerted on it by E_a and the thickness of the barrier layer (or D_b). Since E_b is constant, their concentration inside the barrier layer and near the surface must increase with their concentration at the b/d interface. The latter increases with C_{H2SO4} up to about 2.55 mol dm^{-3}. For

higher C_{H2SO4} values the electrolyte anions concentration in the b/d interface tends to acquire a maximum limiting value, remaining almost independent of C_{H2SO4}. Then, at each h or h/h_c, $n^{1/2}k_{d,a}$ must decrease with C_{H2SO4} up to $\sim$2.55 mol dm^{-3} and, for $C_{H2SO4} >$ 2.55 mol dm^{-3}, $n^{1/2}k_{d,a}$ must acquire a maximum limiting value almost independent of C_{H2SO4}, as indeed shown in Figs. 9 and 10.

On adding $Al_2(SO_4)_3$, electrolyte anions are added in the pore filling solution and a decrease of $n^{1/2}k_{d,a}$ is expected (Figs. 9 and 10). The strong decrease of $n^{1/2}k_{d,a}$ for the $H_2SO_4 + Al_2(SO_4)_3$ (saturated) electrolyte is due mainly to an inhibitory thin $Al_2(SO_4)_3$ precipitate film formed on the pore wall surface and secondarily to the previous reason. The extent of the $n^{1/2}k_{d,a}$ fall is arbitrarily distributed on the surface, justifying the noticeable scatter of points (Fig. 4).

The electrolytes H_2SO_4 (2.55 mol dm^{-3}) and H_2SO_4 (1.53 mol dm^{-3}) + $Al_2(SO_4)_3$ (0.34 mol dm^{-3}) yield comparable total concentrations of both HSO_4^- and SO_4^{2-}. The relevant D_b and E_a values (Table 1) are close. The concentration of HSO_4^- is higher in the first than in the second electrolyte; the opposite is valid for SO_4^{2-}. The SO_4^{2-} ion has a smaller size and higher charge than the HSO_4^- ion and its incorporation must take place more easily and inside deeper layers. Therefore lower $n^{1/2}k_{d,a}$ values should be obtained in the second case. Instead, at each h, and especially at each h/h_c, the $n^{1/2}k_{d,a}$ values are comparable (Figs. 9 and 10). So, the concentration of the incorporated anions in the barrier layer is independent of their kind. This means that, inside the double layer, decomposition of HSO_4^- to SO_4^{2-} and H^+ occurs, which is favored by the field and the increased pH, the incorporated anions being the SO_4^{2-}.

The concentrations of the main anion HSO_4^- present in the electrolytes H_2SO_4, $NaHSO_4$ and $KHSO_4$ (1.53 mol dm^{-3}) are comparable. The cations H^+, Na^+ and K^+ have strongly different mobilities. The relevant $n^{1/2}k_{d,a}$ values generally differ insignificantly (Figs. 9 and 10); some differences concerning $NaHSO_4$ and $KHSO_4$ are due mainly to some small errors made during the a_{H+} determination. The mobility of cations with identical charge does not affect appreciably the incorporation of anions. At each h (or h/h_c) the $n^{1/2}k_{d,a}$ concerning the $Al(HSO_4)_3$ is much lower than that concerning the above electrolytes. The charge, the heat and number of solvation of the Al^{3+} and the size of the solvated Al^{3+} are all much higher than those of H^+, Na^+ and K^+ [53]. These favor the capture of more anions by the ionic cloud of Al^{3+} and their accumulation in the double layer and incorporation in the barrier layer. Further investigation is needed to fully elucidate the effect of cation charges on their incorporation.

The $n^{1/2}k_{d,a}$ values always tend to come closer when $h \rightarrow h_c$, except for the electrolyte $H_2SO_4 + Al_2(SO_4)_3$ (saturated); significant differences at low h/h_c values diminish at high h/h_c values (Fig. 10). This is due to the fact that around the cell boundaries the local $n^{1/2}k_d$ values are always comparable.

The mechanism of incorporation of electrolyte anions in the barrier layer

The mechanism of incorporation of electrolyte anions can now be described. The barrier layer is a microcrystalline material in nature. The addition of OH^- at the pore base surface, the migration of both O^{2-} and OH^- towards the m/o interface and the relevant processes are more favored at some intercrystallite surface points. Narrow microcrevices between microcrystallites are thus formed with widths comparable to the size of solvated anions. Under the field action, the crevices are densely filled by anions.

The ionic migration processes across the barrier layer may also take place across and/or along the intercrystalline surfaces. The crevices are thus propagated to different directions while, on average, they broaden towards the pore base surface. The field strength at the depth of the crevices increases as it approaches the m/o interface. The H_2O molecules solvating the anions are consumed for the previous processes, which cease after the H_2O depletion.

When crevices are initiated, some are simultaneously propagated while others cease to propagate. A random distribution of their depth thus exists. A maximum possible depth of penetration of electrolyte anions, shorter than the thickness of the barrier layer, may be permitted at each anodization condition, which evidently increases with E_a. As the depth of the crevices increases, their surface density decreases. The average local concentration of incorporated electrolyte anions decreases monotonically towards the m/o interface. Near the pore base surface the oxide is a relatively loose material while near the interface it becomes a more compact, crystalline and pure material, in agreement with earlier results [15].

The bell-like distribution of the concentration of incorporated electrolyte anions across the initially formed flat barrier layer [19] and along a thin layer, with thickness comparable to the microcrystallite sizes, on the pore wall surface of an h_c thickness film [52] can now be explained. After the completion of the anodizing process the specimens are always washed, and some times neutralized [21], to remove the attached highly acidic electrolyte since it reacts with and destroys the oxide to some extent. Contact of H_2O with oxide during its washing occurs only from the surface towards the deeper layers, while the crevices become narrower along this direction. The removal of anions is less effective towards deeper layers and for deeper crevices. A distribution of the depth exists, up to which anion removal is possible. The local electrolyte anion concentration must increase up to some depth inside the barrier layer at which the access of washing H_2O and removal of these anions are possible, then it decreases towards the m/o interface, as indeed observed for washed films [19, 52].

The above electrolyte anion distributions across the barrier layer for unwashed and washed films is valid also for the H_2O molecules solvating the electrolyte

anions. The barrier layer and the pore wall material of the anodic alumina contain a small amount of H_2O (either as H_2O or OH^- and H^+), $<1\%$ w/w [21, 46]. The H_2O in the barrier layer can be attributed to the solvating H_2O together with the migrating OH^- and H^+ across this layer just before the end of the anodization process. The presence of H_2O in the pore wall material is attributed to its existence in the barrier layer, which is transformed to the pore wall material by the mechanism of porous layer growth. According to this mechanism, the barrier layer is shifted towards the Al side, leaving behind it the porous, columnar, cellular layer of the film (Fig. 2).

Interpretation of the deviation of the experimental points for the $H_2SO_4 + Al_2(SO_4)_3$ (saturated) electrolyte from the plots in Figs. 6 and 8 and of the variation of P_a with t

When precipitate is absent, the $C_{Al2(SO4)3}$ inside the pores increases towards the pore bases [43]. For the $H_2SO_4 + Al_2(SO_4)_3$ (saturated) electrolyte, a thin precipitate layer covers the whole pore surface. An additional potential drop across this layer at the pore bases and higher P_a and $P_{a,m}$ are necessary for both the ionic current passage through it and the establishment of suitable OH^- and H^+ concentrations at the b/d interface, satisfying Eqs. 22 and 23. The precipitate lowers a_{H+} at the pore wall oxide/precipitate interface as well as the $n^{1/2}r_{d,a}$ and $n^{1/2}r_{d,a,M}$ values. The deviation of the relevant points (Figs. 6 and 8) is thus explained.

Since $C_{Al2(SO4)3}$ increases with t (or h) inside the pore base region [43], the precipitate thickens and P_a increases for $t > t(P_{a,m})$ (Fig. 1). This causes an increase in temperature [54] and in the solubility of $Al_2(SO_4)_3$, enhancing its removal and controlling the thickness of the precipitate in this region. The anodization process thus continues; otherwise it would have to cease.

The variation of P_a for $t > t(P_{a,m})$ in all other cases (Fig. 1) is attributed to an imperceptible variation of a_{H+} in the pore base region. The increase of the $Al_2(SO_4)_3$ concentration with h and its accumulation in this region [43] may cause the decrease of the H^+ concentration and a_{H+}; this was indeed shown previously [43] for low j values, as here, by a transport analysis. This results in an imperceptible decrease of D_b, an increase in the barrier layer thickness and a slight increase of P_a. For the $NaHSO_4$ and $KHSO_4$ electrolytes, P_a slightly decreases. In these cases the rate of Al^{3+} production inside the pores is the lowest. The Na^+ and K^+ are more mobile than the product Al^{3+}. By the mass and charge transport mechanism, these cations in excess assist the removal of Al^{3+} from the pore base region, causing some imperceptible increase of a_{H+} in this region. Considering the high field strength across the barrier layer, the small variation of P_a for $t > t(P_{a,m})$ in the above cases owing to the change of its thickness shows that D_b is essentially constant.

The slight scatter of points in Figs. 5 and 8 is due to errors made in the determination of nD_b^2 and a_{H+} and to differences between the H^+ concentration and a_{H+} at pore bases and those in the bath which were taken into consideration. This scatter is also due to some variation of the H^+ concentration and a_{H+} in the bath and therefore in the pore base region during anodizing, because the rate of H^+ discharge in the cathodes is higher than that of H^+ production at the pore bases [43]. This is also partially due to the fact that the $r_{d,a,M}$ values are not exactly what they should be at $t = t_t$ and may differ slightly from the real average ones. Accurate a_{H+} values and their distribution along the pores can be found by a mass and charge transport analysis [43], which is complex and out of the scope of this study. The experimental points concerning the electrolyte H_2SO_4 (4.59 mol dm^{-3}) in Figs. 5 and 8 fall essentially on the plots. Hence the estimation made for a_{H+} in this solution is indeed valid.

An important question still remaining unanswered is the mechanism of the appearance and development of the barrier layer in the form of a close-packed array of hemispherical shell units at the initial stages of anodization, yielding the porous structure. During oxidation the initial volume of Al expands. Significant mechanical stresses may develop as, for example, during the oxidation of Fe [55, 56]. This mechanism may be revealed in future studies on the basis of both the anticipated physicochemical processes and the mechanical stresses involved.

Conclusions

The results in this study may introduce much significant information into the topic of Al anodization, stimulating further research and applications. Among the direct consequences of these results in the production of porous anodic films in the electrolytes employed here, and their properties and applications, the following are noted:

1. The acceleration of oxide dissolution across the pore walls towards the cell boundaries during anodizing predicts that, for constant or slightly variable composition and temperature of electrolyte along the pores, the real pore shape must be that of an elongated trumpet.
2. For identical H_2SO_4 concentrations, films formed in $H_2SO_4 + Al_2(SO_4)_3$ electrolyte have lower porosity than those formed in H_2SO_4 alone and the growth of hard films is favored only for thick films; the opposite is valid for thin films (Fig. 4).
3. The processes taking place on the pore base and pore wall surfaces and their mechanisms may be used to predict methods to obtain desired pore base diameters and the opening up of pores, high porosity or real surfaces, e.g. for catalysis applications [28, 29, 30, 31, 32, 33 , 34], or low porosity, e.g. for applications of hard films.

4. The mechanism of incorporation of electrolyte anions and their real distribution across the barrier layer may be used to predict methods for a controlled/designed implantation of anions carrying catalytically active species. Thus the development of ultra-active catalysts or supports of designed porous structure will become possible.
5. Generally, the design of the structure, the improvement of properties and the predictions of new scientific and technological applications of these aluminas appear now to be possible.

Among the further consequences of the discovered physicochemical processes and mechanisms in the research of the entire topic of Al anodization, the following are noted:

1. The role of sulfate additives in the growth of hard films [35, 36, 37, 38] can now be explained.
2. The discovered processes and mechanisms may shed light towards the elucidation of the mechanism of pitting appearance [39] and the role of sulfates [7, 35]; methods may be devised to produce regular films even in conditions where, otherwise, pitting would appear.
3. On the basis of the above mechanisms, the peculiar processes and mechanisms during the growth of films in other pore forming electrolytes may be revealed.
4. With their aid, the mechanism by which the initial flat barrier layer is transformed to the close packed array of hemispherical shell units, yielding the development of a porous film with a characteristic structure, may be revealed. This will give rise to further investigations on the properties and applications of porous anodic alumina films.

References

1. Young L (1961) Anodic oxide films. Academic Press, London
2. Diggle JW, Downie TC, Goulding CW (1969) Chem Rev 69:365
3. Nagayama M, Tamura K (1967) Electrochim Acta 12:1097
4. Nagayama M, Tamura K (1968) Electrochim Acta 13:1773
5. Nagayama M, Tamura K, Takahashi H (1970) Corros Sci 10:617
6. O'Sullivan JP, Wood GC (1970) Proc R Soc (London) Ser A 317:511
7. Wood GC, O' Sullivan JP (1970) Electrochim Acta 15:1865
8. Siejka J, Ortega C (1972) J Electrochem Soc 124:883
9. Neufeld P, Ali HO (1973) J Electrochem Soc 120:479
10. Diggle JW (1973) Electrochim Acta 18:283
11. Diggle JW, Downie TC, Goulding CW (1970) Electrochim Acta 15:1079
12. Keller F, Hunter MS, Robinson DL (1953) J Electrochem Soc 100:411
13. Renshaw TA (1961) J Electrochem Soc 108:185
14. Leach JSL, Neufeld P (1969) Corros Sci 9:413
15. Thompson GE, Furneaux RC, Wood GC (1978) Corros Sci 18:481
16. Furneaux RC, Thompson GE, Wood GC (1978) Corros Sci 18:853
17. Takahashi H, Nagayama M (1978) Corros Sci 18:911
18. Treverton JA, Davies NC (1980) Electrochim Acta 25:1571
19. Parkhutic VP (1986) Corros Sci 26:295
20. Dell'Oca CJ, Fleming PJ (1976) J Electrochem Soc 123:1487
21. Patermarakis G, Lenas P, Karavassilis CH, Papayiannis G (1991) Electrochim Acta 36:709
22. Patermarakis G, Tzouvelekis D (1994) Electrochim Acta 39:2419
23. Shreir LL (1976) Corrosion, vol. 2. Newnes-Butterworths, London
24. Kawai S, Ueda R (1975) J Electrochem Soc 122:32
25. Kawai S (1975) J Electrochem Soc 122:1026
26. Kawai S, Ishiguro I (1976) J Electrochem Soc 123:1047
27. Smith AW (1973) J Electrochem Soc 120:1068
28. Rai K, Ruckenstein E (1975) J Catal 40:117
29. Chu Y, Ruckenstein E (1976) J Catal 41:384
30. Ihm SK, Ruckenstein E (1977) J Colloid Interface Sci 61:146
31. Ihm SK, Ruckenstein E (1978) Ind Eng Chem Prod Res Dev 17:110
32. Patermarakis G, Pavlidou C (1994) J Catal 147:140
33. Patermarakis G, Moussoutzanis K, Chandrinos J (1999) Appl Catal A 180:345
34. Patermarakis G, Nicolopoulos N (1999) J Catal 187:311
35. Fukuda Y, Fukushima T (1983) Electrochim Acta 28:47
36. Mason RB (1956) J Electrochem Soc 103:425
37. Tajima S, Umehara Y (1981) Plating Surf Finish 68:54
38. Tomita S (1981) Alutopia 11(4):15
39. Patermarakis G, Moussoutzanis K (2001) Corros Sci 43:1433
40. Patermarakis G, Moussoutzanis K (1995) J Electrochem Soc 142:737
41. Dodos D (1975) Electrochemical data. Elsevier, Budapest
42. Patermarakis G, Moussoutzanis K (1995) Electrochim Acta 40:699
43. Patermarakis G (1998) J Electroanal Chem 447:25
44. Brunnelle JP (1978) Pure Appl Chem 50:1211
45. Kasztelan S, Payen E, Toulhoat H, Grimblot J, Bonnelle JP (1986) Polyhedron 5:157
46. Patermarakis G, Kerassovitou P (1992) Electrochim Acta 37:125
47. Baker B, Pearson R (1972) J Electrochem Soc 119:160
48. Ono S, Ichinose H, Masuko N (1991) J Electrochem Soc 138:3705
49. Weast RC (ed) (1980) Handbook of chemistry and physics, 60th edn. CRC Press, Boca Raton, p F-214
50. Sanderson RT (1976) Chemical bonds and bond energy, 2nd edn. Academic Press, New York
51. Cabrera N, Mott NF (1948) Rep Prog Phys 12:163
52. Patermarakis G, Moussoutzanis K, Nikolopoulos N (1999) J Solid State Electrochem 3:193
53. Antropov L (1972) Theoretical electrochemistry. Mir, Moscow
54. Applewhite FR, Leach JSL, Neufeld P (1969) Corros Sci 9:305
55. Batis G, Routoulas A (1999) Cement Concrete Composits 21:163
56. Routoulas A, Batis G (1999) Anti-Corros Methods Mater 3:276